ACS OMEGA

http://pubs.acs.org/journal/acsodf

Article

Detecting Phytoplankton Cell Viability Using NIR Raman Spectroscopy and PCA

Nina I. Novikova,* Hannah Matthews, Isabelle Williams, Mary A. Sewell, Michel K. Nieuwoudt, M. Cather Simpson, and Neil G. R. Broderick

Cite This: *ACS Omega* 2022, 7, 5962−5971

Read Online

ACCESS | Metrics & More | Article Recommendations

ABSTRACT: Raman spectroscopy has long been suggested as a potentially fast and sensitive method to monitor phytoplankton abundance and composition in marine environments. However, the pitfalls of visible detection methods in pigment-rich biological material and the complexity of their spectra have hindered their application as reliable *in situ* detection methods. In this study we combine 1064 nm confocal Raman spectroscopy with multivariate statistical analysis techniques (principle component analysis and partial leas-squares discriminant analysis) to reliably measure differences in the cell viability of a diatom species (*Chaetoceros muelleri*) and two haptophyte species (*Diacronema lutheri* and *Tisochrysis lutea*) of phytoplankton. The low fluorescence background due to this combined approach of NIR Raman spectroscopy and multivariate data analysis allowed small changes in the overall spectral profiles to be reliably monitored, enabling the identification of the specific spectral features that could classify cells as viable or nonviable regardless of their species. The most significant differences upon cell death were shown by characteristic shifts in the carotenoid bands at 1527 and 1158 cm^{-1}. The contributions from other biomolecules were less pronounced but revealed changes that could be identified using this combination of techniques.

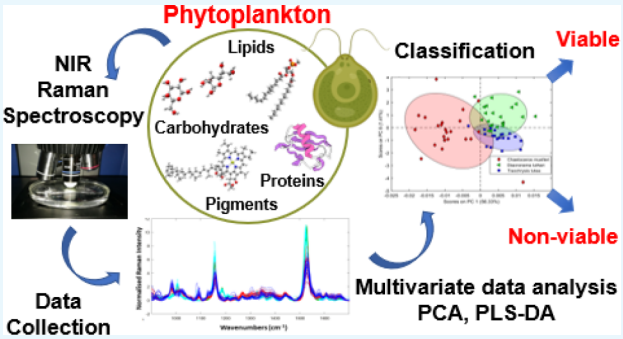

INTRODUCTION

Phytoplankton form the base of the aquatic food chain and are responsible for almost half the gross primary production on earth.[1] The state of marine phytoplankton communities is of great importance ecologically as well as in aquaculture, where the productivity, quality, and safety of products are directly and critically affected by natural phytoplankton communities.[2] Phytoplankton contain a rich variety of biomolecules such as lipids, proteins, carbohydrates, and biosilicates that serve as the primary nutrient and mineral sources as well as pigments such as chlorophyll and carotenoids that facilitate photosynthesis. Recent reports on climate change projections show that expected changes in temperature, pH, and salinity will have a significant impact on the marine environment, including phytoplankton localization, population, and biodiversity.[3] It is therefore crucial to monitor phytoplankton communities to track environmental impacts, maintain productivity in the aquaculture sector (*e.g.*, mussel farms), and facilitate developments in other emerging industrial applications, such as the biofuel industry.

Current methods of phytoplankton detection range from global monitoring such as seasonal algae bloom tracking using satellite and hyperspectral imaging to more precise localized methods such as fluorescence spectroscopy, PCR, HPLC, mass spectrometry, and flow cytometry, which give information on abundance and variability in the population.[4,5] Fluorescence spectroscopy is a rapid, low cost, and highly sensitive method as it easily detects small concentrations of chlorophyll and other pigments. However, it is not very specific and is generally used to either approximate total plankton concentrations or detect the presence of species that have the potential to cause harmful algae blooms (HABs).[6] PCR, HPLC, mass spectroscopy, and flow cytometry, on the other hand, are techniques that provide information-rich quantitative data that can be used to monitor factors such as the diversity and health of the phytoplankton population as well as to identify specific toxins.[7−10] These methods are very precise but are lab-based and time-consuming, require trained personnel to do extensive sample preparation and complicated data analysis, and expensive as a result. In many cases these methods do not allow the rapid detection required for immediate intervention

Received: November 7, 2021
Accepted: January 28, 2022
Published: February 10, 2022

Table 1. Phytoplankton Division, Class, and Genus and a List of Major Chlorophylls and Carotenoids

division	class	genus and species	chlorophylls	major carotenoids
Haptophyta	Prymnesiophyceae	*Tisochrysis lutea*	Chl a and c (c_1 and c_2)[29]	fucoxanthin, diadinoxanthin, β-carotene, diatoxanthin, and echinenone[30]
	Pavlovophyceae	*Diacronema lutheri*	Chl a and c[29]	fucoxanthin, β-carotene, and canthaxanthin[31]
Ochrophyta	Bacillariophyceae	*Chaetoceros muelleri* (diatom)	Chl a and c[32]	fucoxanthin, diadinoxanthin, β-carotene, and diatoxanthin[33]

in vast dynamic environments such as coastal or open ocean waters.

More recently Raman spectroscopy was proposed as an alternative method to monitor the health of phytoplankton populations.[11] This technique measures complex molecular signatures and has the potential to be label-free, rapid, and highly specific, requiring limited sample preparation and allowing real-time detection *in situ*. This is due to the inherently low interference from water, the sensitivity to crucial biomolecules, and recent technological advancements in laser and optics technologies and data analysis methods.[12] In addition, a large amount of literature is now available that reports the detailed assignment of Raman bands for a vast library of important biomolecules. In most cases these biomolecules were either synthetically prepared or extracted from biological systems, making these data a useful starting point for complex *in situ* Raman band identification.[13,14]

A proof of concept has already shown use of visible Raman spectroscopy to identify species and monitor parameters such as the stress-induced nutrient depletion, lipid content, and cell viability of phytoplankton.[11,15−18] Current reports, however, highlight significant limitations that prevent a broader application of this method. One issue arises from the fluorescence exhibited by marine phytoplankton, which can result in weaker Raman signals being either masked by or superimposed on a strong fluorescent background.[19] To mitigate this, extensive data preprocessing steps are employed that can easily degrade the data integrity if not applied carefully. Strong fluorescence upon Raman excitation in the visible region is unavoidable due to emission from the photosynthetic pigments naturally present in these organisms.[20,21] In addition, the pigment bands tend to dominate the spectra due to resonance enhancement with a large range of wavelengths in the visible region, while no such enhancement occurs in bands from the other biomolecules, such as fats and proteins.[22] This means that crucial spectral information about the components of interest can be drowned out or masked by the large background signals from the more Raman-active chromophores.

A second obstacle to the application of Raman spectroscopy for phytoplankton analysis is the complexity of the resultant spectra. Phytoplankton cells have a highly multicomponent biomolecular composition. To address this issue, statistical multivariate analysis methods, which have been successfully applied in other complex systems, have been proposed.[23−25] To date, however, literature on the application of chemometric methods for phytoplankton Raman analysis is limited to reports on nutrient composition or depletion, the detection of invasive problematic phytoplankton species, and one report on cell viability.[11,17,18] These studies showed the great potential of Raman spectroscopy but suffered from the limitations mentioned above and the reported limited application of chemometric methods, which hindered the identification of broader trends in the complex Raman spectra of phytoplankton.

A recently published study by Gordon et al.[26] showed that a combination of FT-IR and FT-Raman spectroscopy with NIR excitation can be used conjointly with multivariate data analysis to differentiate *Lindavia intermedia*, a diatom responsible for lake snow (a costly nuisance in fresh water), from several other algal taxa. This study highlighted the potential for vibrational spectroscopy with NIR excitation as a fast and reliable tool in phytoplankton monitoring applications.

In this work we demonstrate the use of confocal Raman spectroscopy with NIR excitation to provide a stand-alone spectroscopic method for the assessment of phytoplankton cell viability. Prior to the Raman analysis, excitation measurements were used to monitor changes in the pigment environment and track the cell viability. Using excitation at 1064 nm avoided the fluorescence commonly exhibited by these organisms, thus enabling the measurement of unique chemical signatures in both viable and nonviable cells of three phytoplankton species with very similar pigment profiles. Using principal component analysis (PCA) of the Raman spectra, the differences between species and the cell viability could be revealed and assessed through minor differences in their spectral components. Partial least-squares discriminant analysis (PLS-DA) was additionally used as a classification method to determine the accuracy of the cell viability assignment. Finally, an assessment of the loading vectors obtained from the PCA provided useful spectral indicators that could be used to monitor phytoplankton population health on-site using future portable devices.

RESULTS AND DISCUSSION

Pigment Composition. The three phytoplankton species reported in this work are *Tisochrysis lutea* (*T. lutea*), *Diacronema lutheri* (*D. lutheri*), and *Chaetoceros muelleri* (*C. muelleri*). Both *T. lutea* and *D. lutheri* are golden brown flagellated microalgae of the same division but different classes (Haptophyta and Prymnesiophyceae, respectively). *C. muelleri*, on the other hand, is a centric diatom of the division Ochrophyta in the class Bacillariophyceae (Table 1). The three phytoplankton species contain chlorophyll a and c as common photosynthetic pigments and fucoxanthin (Fx) as an abundant carotenoid but differ in the composition of other major carotenoid pigments (Table 1). Fx is an important pigment that acts as a light-harvesting antenna and photoprotecting agent in a Fx−chlorophyll a or c binding protein (FCP). FCP is at the center of photosystem two (PSII) of many microorganisms and attracts significant attention due to its role in highly abundant diatoms and microalgal species that play a significant role in global primary productivity.[27] Fx absorbs in the blue-green region of the visible spectrum not covered by the absorption of chlorophyll and is responsible for the yellow or brown color of the phytoplankton. Fx is regarded as an efficient energy transfer agent that directs the absorbed energy to the chlorophyll and helps dissipate the energy to prevent photodamage. Diadinoxanthin (Ddx) is another carotenoid thought to be important to PSII and has been

https://doi.org/10.1021/acsomega.1c06262
ACS Omega 2022, 7, 5962−5971

suggested to also play a crucial role in energy dissipation in this PSII assembly.[28]

Changes in Excitation Spectra Due to Cell Viability. Heat treating the phytoplankton cells did not result in cell lysis, but a color change from a golden brown mixture to a greener mixture was observed in all samples. To assess the cell viability and measure changes in the pigment composition and environment, excitation spectra of each sample were taken before and after the heat treatment (Figure 1). This technique

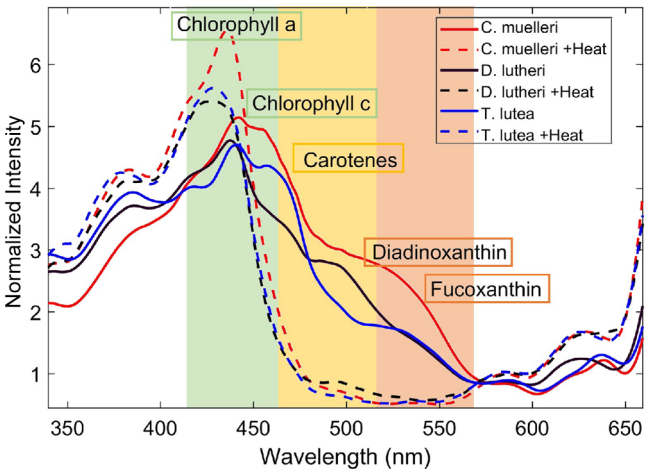

Figure 1. Excitation spectra at $\lambda_{(max)}$ = 680 nm fluorescence of viable and heat-treated cells of the three phytoplankton organisms (*C.muelleri*, *T. lutea*, and *D. lutheri*). The regions of absorption for some common pigments are indicated on the graph.

was chosen for two reasons: (1) the very low background interference when compared to that of UV−Vis absorption spectroscopy of a phytoplankton cell suspension in seawater and (2) the ability to gain information about pigment organization and energy transfer between carotenoids and chlorophyll assemblies in photosynthetic proteins. Visible light emission of the phytoplankton taxa measured here occurred at $\lambda_{(max)}$= 680 nm due to the presence of chlorophyll a and c. Excitation spectra of the phytoplankton were therefore recorded for emission at this wavelength. Fluorescence of the free carotenoid molecules is generally observed in the 500−650 nm range and is heavily dependent on the type of carotenoid pigment present. Energy transfer from carotenoids to chlorophyll occurs when the pigments are assembled in the protein structure. Therefore, fluorescence from chlorophyll is observed when carotenoid pigments in those assemblies absorb light, while the carotenoid fluorescence is quenched. This can be seen in the excitation spectra of viable cells (Figure 1). Absorption bands between 450−550 nm are characteristic of carotenoids, specifically Fx, Ddx, and β-carotene. Once the sample is heat-treated, those bands disappear, and emission at 680 nm only occurs upon excitation at 450 nm or below and in the Q bands of the chlorophyll in the red region, (*i.e.*, chlorophyll absorption). This is a consequence of one or a combination of several of the following processes: (1) denaturation of the tertiary protein structure around the pigment assembly, which allows pigments to lose their ability to transfer energy through normal pathways; (2) isomerization of the carotenoid molecules, which achieves the same result; or (3) preferential degradation of the carotenoid molecules. The occurrence of any of these three processes results in a disruption of the vital processes in the phytoplankton cells and is used as an indicator of cell viability. This can provide a potentially simple method for detecting general changes to the phytoplankton cell viability that can be combined with fluorescence spectroscopy for bulk sample analysis.

Raman Spectra Assignment. Raman spectra recorded with 1064 nm excitation gave a low fluorescent background (Figure 2). This allowed long acquisition times to be used in

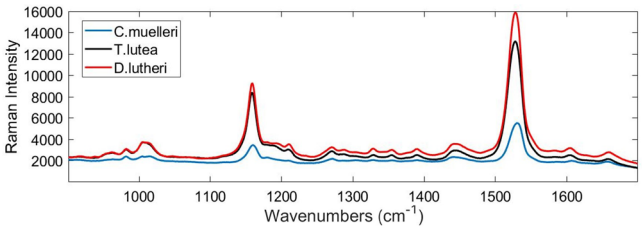

Figure 2. Averaged raw Raman spectra of three phytoplankton species (*C. muelleri*, *T. lutea*, and *D. lutheri*).

combination with high irradiation powers, and no observable pigment bleaching occurred. The spectra obtained were reproducible with broad but well-defined and consistent peaks, allowing small spectral changes to be monitored accurately and reliably.

Figure 3 shows the mean averaged, peak normalized spectrum of the three phytoplankton species. A brief list of peak assignments is given in Table 2.

The Raman spectra of all phytoplankton measured are strongly dominated by carotenoid pigment bands at 1157−1158 cm^{-1} (C−C stretching) and 1527 cm^{-1} (C═C stretching). The 1527 cm^{-1} band is very broad, indicating the presence of a complex mixture of carotenoids that is typical of phytoplankton cells. Extensive studies of the carotenoid Raman shifts observed in microorganisms have previously shown that the main carotenoid Raman peak position can vary from 1504 to 1535 cm^{-1}.[20] Typical Fx and Ddx signals appear at 1529 cm^{-1}. The signal of diatoxanthin is very close in position at 1527 cm^{-1}, while α- and β-carotene signals appear at significantly lower wavenumbers (1521 cm^{-1}).[20] However, the β-carotene band has been detected within a wide wavenumber range (1514−1524 cm^{-1}), differing in position among species of phytoplankton. Fx is the major contributor to the components observed in the spectra of the three phytoplankton studied here; however, contributions from other carotenoids are likely responsible for the broad profile of this band. The broad profile could be further complicated by the presence of Fx isomers with one or more C═C bonds in cisoid configuration. A recent report of the X-ray structures of PSII in diatoms shows that the Fx pigment exists in several conformations in the FCP matrix.[28]

The 1140−1220 cm^{-1} region more clearly shows mixed spectral contributions, as evidenced by the complexity of the peak pattern surrounding the 1157−1158 cm^{-1} band. The bands in this region are assigned as C−H and N−C modes of carotenoids, with weaker contributions from chlorophyll. This complexity is typical of Raman profiles of carotenoid mixtures with the presence of different *cis*−*trans* isomers.[37] The main band in this region (1158 cm^{-1}) is noticeably shifted in position in the spectra of the diatom (*C. muelleri*) compared to those of the other microalgal phytoplankton. This indicates differences in the carotenoid composition among the three

https://doi.org/10.1021/acsomega.1c06262
ACS Omega 2022, 7, 5962−5971

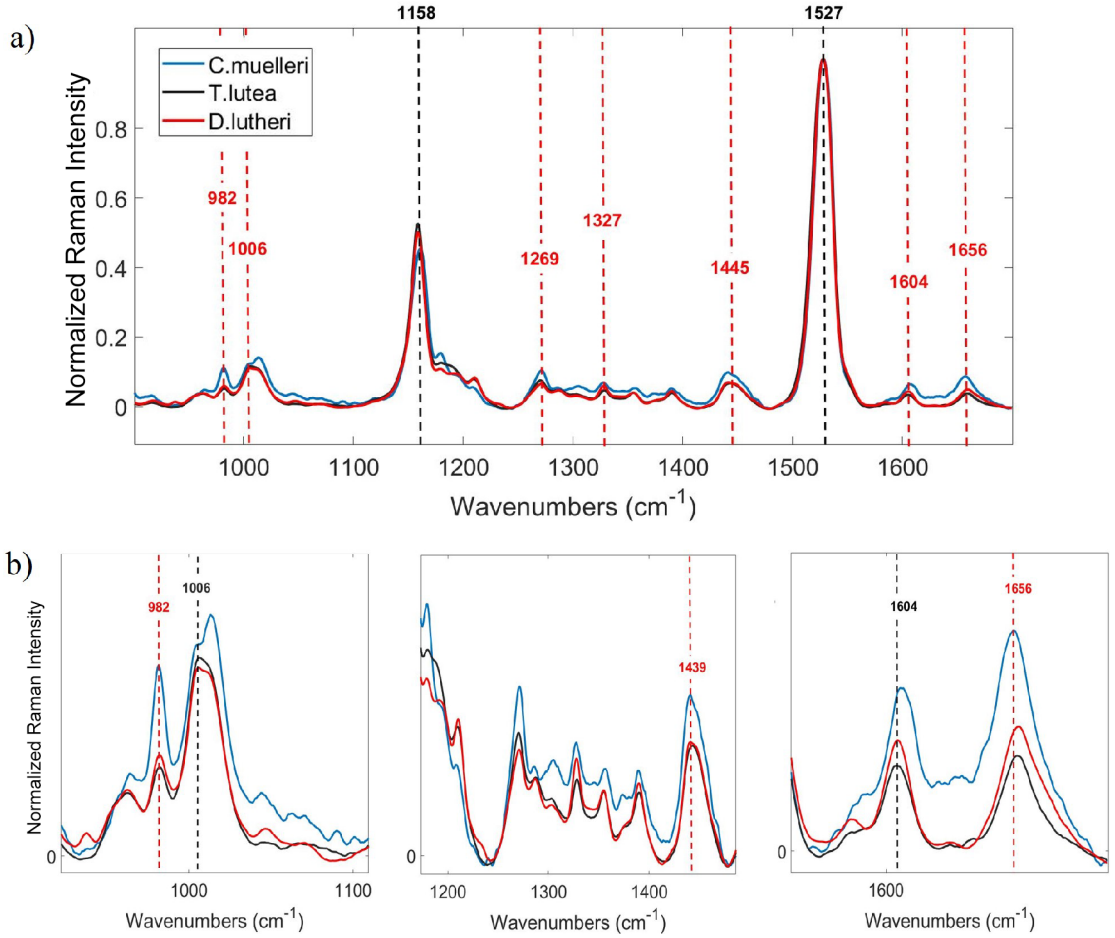

Figure 3. (a) Mean-averaged and peak-normalized Raman spectra of three phytoplankton species (*C. muelleri*, *T. lutea*, and *D. lutheri*), which are normalized to the peak at 1527 cm^{-1}. (b) Enlarged view of the lower-signal-intensity regions highlighting the differences in spectral features among the three species.

Table 2. Main Raman Bands of the Phytoplankton Spectra

Raman shift (cm^{-1})	assignment	biomolecule	ref
1656	C=C stretching, amide 1, and N−C=O stretching	unsaturated lipids, proteins, and chlorophyll	34 and 35
1604	C=C stretching	chlorophyll	35
1527	C=C stretching	carotenoids and chlorophyll	20, 35, and 36
1440−1445	C−H_2 deformations	lipids, proteins chlorophyll, and carbohydrates	34 and 35
1250−1400	C−H_2 deformations, amide III C−N stretching, and N−H deformations	lipids, proteins, chlorophyll, carbohydrates, and carotenoids	34−36
1158	C−C stretching	chlorophyll and carotenoids	20, 35, and 36
1006	C−CH_3 stretch	carotenoids and proteins	20, 34, and 36
970−1004	C−C stretching and =CH stretching	proteins, lipids, carotenoids, and chlorophyll	34−36

species and supports the conclusion that other carotenoid pigments are contributing to the Raman spectral bands.

The band at 1006 cm^{-1} is a C−CH_3 stretching mode that is located in another complex region with signals in the 1000−1015 cm^{-1} range, which is also typical of carotenoid bands. The signals are likely broadened due to peak overlap with Raman bands from nonpigment contributions, including breathing modes of the phenylalanine ring in protein structures and other aromatic nucleic acids.[38] The peaks at 1445 (C−CH_2 bend) and 1656 cm^{-1} (C=C stretch) are characteristic of protein and lipid contributions and indicate the presence of saturated and unsaturated fats, respectively.[39] Chlorophyll peaks are not as pronounced as carotenoid peaks; however, the signals at 1269, 1327, and 1604 cm^{-1} are all indicative of chlorophyll a.[38] In addition, the broad bands at 1527 and 1158 cm^{-1} are expected to contain contributions from chlorophyll a and c and the carotenoids, although the chlorophyll signals are much weaker at this excitation wavelength.

The central region of the spectral window (1250−1500 cm^{-1}) contains broad signals from the strongly overlapped contributions of a wider range of biomolecules, including lipids, proteins, and carbohydrates. This region is typically hard to analyze due to the low intensities of the overlapping peaks with broad profiles, which can be easily lost or skewed in the preprocessing steps as they can be masked by the large fluorescent background. However, the use of 1064 cm^{-1} NIR excitation minimized the fluorescence background and allowed these spectral features to be distinguished. Finally, the peak at 982 cm^{-1} is due to the media in which the phytoplankton were cultured.

Discrimination of Three Phytoplankton Species. The variance in the data matrix of the spectral profiles of the three phytoplankton species was analyzed using PCA. The majority

https://doi.org/10.1021/acsomega.1c06262
ACS Omega 2022, 7, 5962−5971

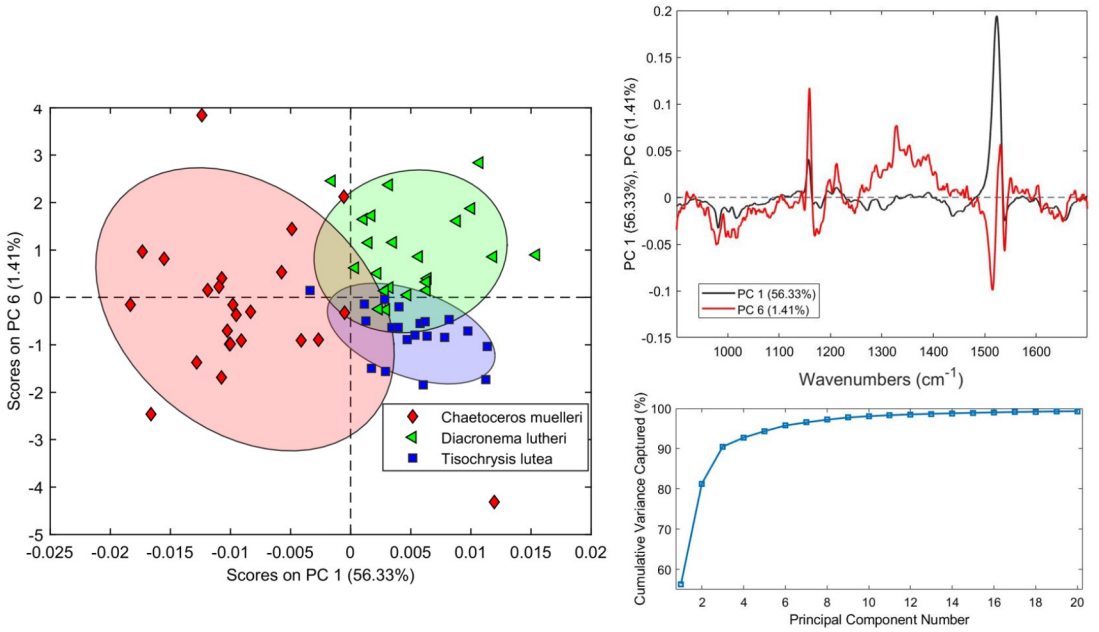

Figure 4. Plot of PC1 vs PC6 scores and the respective loading plots from the PCA of both the viable and heat-treated cells of three phytoplankton species, with confidence ellipses at the 80% confidence interval and a cumulative variance contribution rate curve for the first 20 principle components.

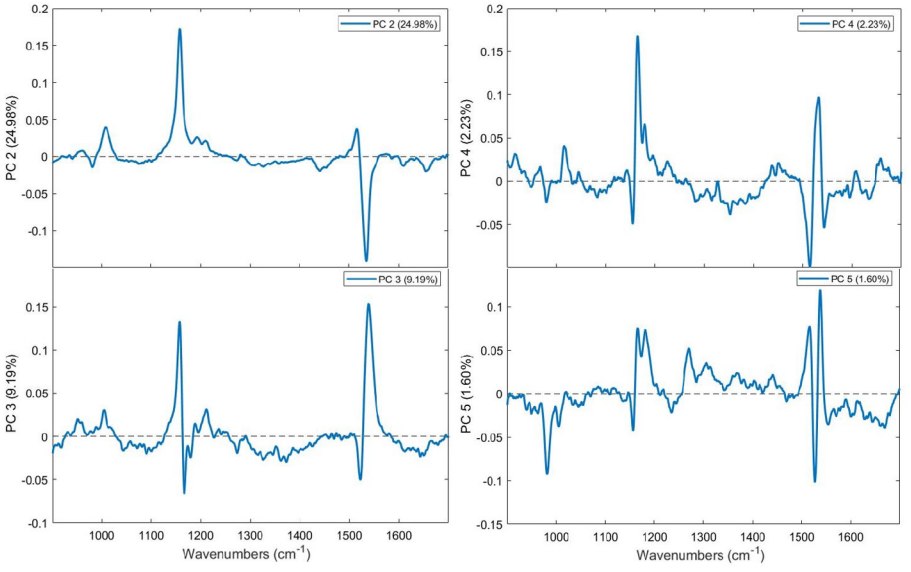

Figure 5. PC2, PC3, PC4, and PC5 loading plots from the PCA of viable and nonviable cells of three phytoplankton species.

of the variance (96%) can be explained using six principal components. Principal component (PC) 1 describes differences in the overall intensity of the Raman spectra and in many aspects mirrors the raw Raman spectra. However, despite having very similar Raman spectra and pigment compositions, the three species can be clearly distinguished from each other using PC1 and PC6 (Figure 4).

PC1 and PC6 represent 56% and 1.4% of the variance, respectively. The scores and loadings for the two components are shown in Figure 4. The diatom (*C. muelleri*), which has negative PC1 scores, is clearly separated from the positive-scoring *T. lutea* and *D. lutheri*. Spectral loadings for PC1 indicate that significant variance comes from the intensity difference of the 1158 cm^{-1} band. This is a C−C band in the carotenoid pigment and might indicate that the pigments present, and their environment in the diatom, are significantly different from those in the haptophytes. This is not surprising considering that diatoms were shown to have originally evolved differently than haptophytes. Thus, they are expected to have different protein and pigment assemblies.[40] In addition, *C. muelleri* shows stronger signals for lipid and protein bands compared to *T. lutea* and *D. lutheri*, which is most clearly visible in the 1658 and 1445 cm^{-1} regions. The chlorophyll, carotenoid, and protein contributions in the regions around 1006 and 1250−1400 cm^{-1} show differences between the species. *C. muelleri* is known to have a high lipid content and has elicited interest in applications such as biofuels.[41] The higher lipid content in this diatom could explain the observed differences.

https://doi.org/10.1021/acsomega.1c06262
ACS Omega 2022, 7, 5962−5971

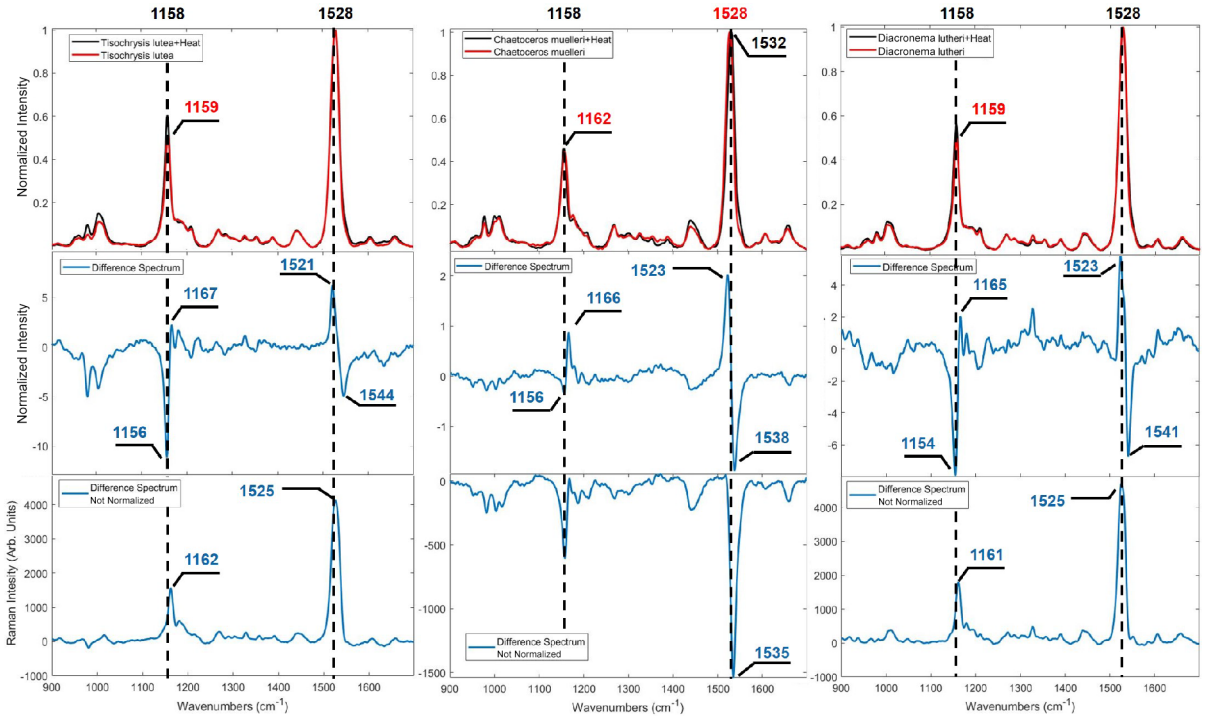

Figure 6. Peak-normalized and averaged Raman spectra of viable (red) and heat-treated (black) *T. lutea*, *C. muelleri*, and *D. lutheri* phytoplankton cells and their difference spectra before and after normalization (blue).

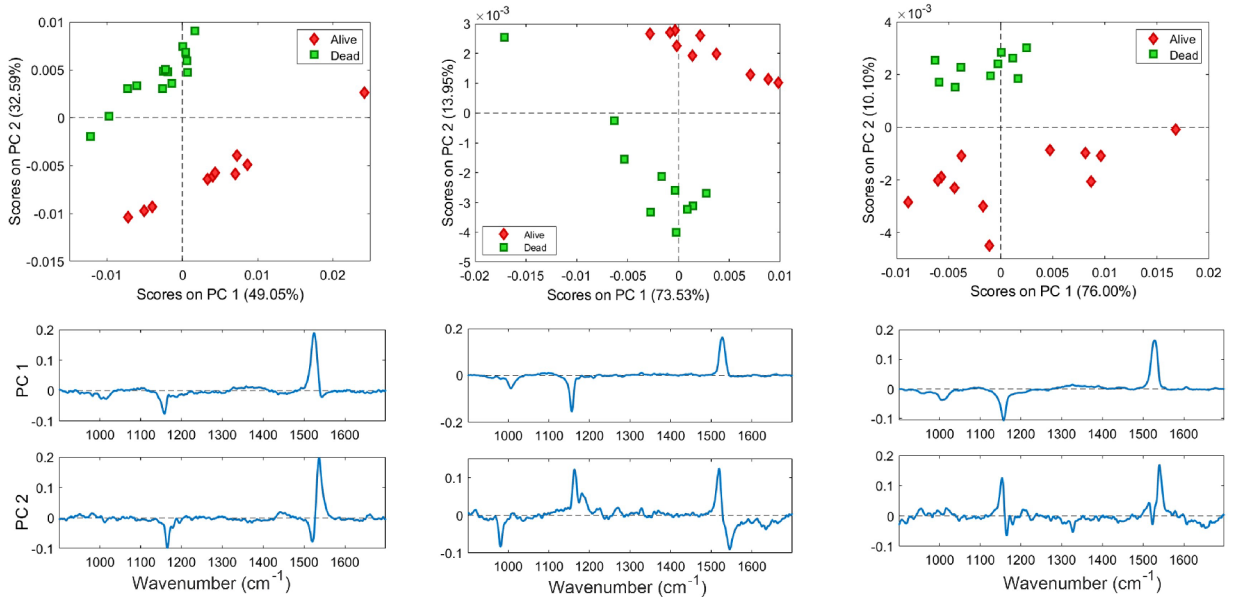

Figure 7. Plots of PC1 vs PC2 scores and the respective loading plots from the PCA of the viable and heat-treated cells of *C. muelleri*, *T. lutea*, and *D. lutheri* (left to right).

The two haptophytes can also be distinguished from each other as they differ in their PC6 scores. Overall, *D. lutheri* scores positively in PC6 while *T. lutea*s scores negatively. From the PC6 loading, the main difference between the two species can be seen in the slight peak shifts of the two main carotenoid bands at 1527 and 1158 cm^{-1}. Also significant is the 960 to 1450 cm^{-1} range. PCA therefore enabled the identification of the two species based mainly on differences in their carotenoid compositions, which were not immediately obvious in the raw NIR Raman spectra (Figure 5).

Cell Viability Assessment Using PCA and PLS-DA. Peak-normalized and averaged Raman spectra of fresh and heat-treated *T. lutea*, *C. muelleri*, and *D. lutheri* samples, as well as the corresponding difference spectra before and after normalization, are shown in Figure 6. To obtain the difference spectrum, an average spectrum of the viable cells was subtracted from the spectrum of heat-treated cells. Subtraction was carried out in a 1:1 ratio of normalized and non-normalized spectra, and no internal Raman band was used as a standard.

https://doi.org/10.1021/acsomega.1c06262
ACS Omega 2022, 7, 5962−5971

Upon heat treatment, the 1528 cm^{-1} carotenoid band shifted significantly to higher wavenumbers, while the 1162 cm^{-1} band shifted slightly to lower wavenumbers. In addition, the relative band intensities of these two bands changed significantly, with the 1528 cm^{-1} band losing intensity relative to the 1162 cm^{-1} band. This could be indicative of (1) changes to the carotenoid molecule such as the C−C isomerization of one of the long conjugated chains or (2) changes in the relative caratenoid composition due to degradation. Other features of note are the lipid bands around 1656 and 1445 cm^{-1}, which are distinct in nonviable cells compared to fresh samples in *C. muelleri*. This was not observed in the two haptophyte samples, although there were low-intensity bands present in the difference spectra of those regions. This is attributed to a higher signal-to-noise ratio obtained for *C. muelleri*, possibly due to the higher lipid content present in this genus as suggested previously.

Each phytoplankton type was individually analyzed using PCA, and scores and loadings are shown in Figure 7. Viable and nonviable cells can be easily separated using scores from only two principal components. These two principal components are dominated by the same two carotenoid peaks in all three species and explain the majority of the variation, with an 82% contribution in *C. muelleri*, an 88% contribution in *T. lutea*, and an 86% contribution in *D. lutheri*. PC1 mostly describes relative intensity changes between the two main carotenoid peaks discussed above. This shift can be explained by *trans*−*cis* isomerization in the carotenoid structure, differential thermal degradation that results in changes in the relative concentrations of different carotenoids, or the denaturation of protein structures. The viable and nonviable cells are not clearly separated by PC1 scores alone, especially for the *D. lutheri* species, which shows that cell viability is independent of PC1. PC2 adds enough information to clearly separate the cell viability for all species, as viable cells in *C. muelleri* and *D. lutheri* score low on PC2 while *T. lutea* shows an opposing trend.

As seen in the loadings of PC2 compared to those of PC1 for *C. muelleri*, Figure 8 highlights the change in position of the main carotenoid peaks. The two main carotenoid peaks shift from the PC1 loading to the PC2 loading, indicating different carotenoid contributions to each PC. Similar to phytoplankton species differentiation, the majority of the spectral variation is explained by the carotenoid signals, with an additional minor contribution from lipid bands at higher PCs.

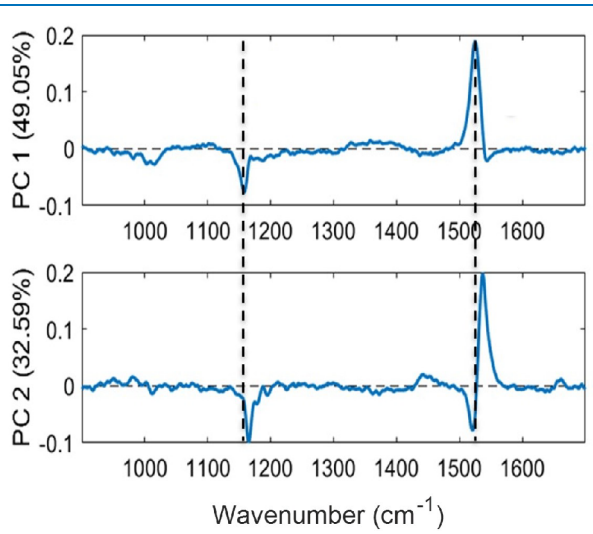

Figure 8. PC1 vs PC2 loadings from the PCA of the viable and heat-treated cells of *C. muelleri*.

PLS-DA was used to classify the samples as viable or nonviable independent of the type of phytoplankton. All 66 samples were used in the PLS-DA model and were split into a calibration set (2/3) and an external validation set (1/3). The model threshold for classifying viable versus nonviable samples was selected by finding the optimum sensitivity and specificity for both of the modeled classes. The model thresholds were thus selected as 0.53 for the viable cells and 0.47 for the nonviable cells (Figure 9).

A two-component model with a random cross validation showed the excellent classification of viable and nonviable cells. The cross validation misclassified one sample from the *D. lutheri* group as nonviable, while the external validation set classified all samples correctly. The sensitivity and specificity from cross validation were both ≥95%, while for the external validation set both the sensitivity and specificity were 100%. The one spectrum of *D. lutheri* that was misclassified as dead could in fact have been correctly classified, as it was not possible to control plankton cells dying of natural causes in the live samples. The latent variable loadings (Figure 10) also show that regions of the spectrum similar to those identified with PCA were used to classify viable and nonviable cells.

CONCLUSION

In this work we showed that the combination of NIR Raman spectroscopy with multivariate data analysis provides an excellent tool for the classification and viability assessment of phytoplankton in marine environments. We have demonstrated the ability of these techniques to successfully differentiate among species with very similar pigment profiles and to also identify viable versus nonviable cells irrespective of species. Small shifts and ratio differences in the major carotenoid bands reflected changes in the environments of the biomolecules present in the cell upon cell death that were independent of the phytoplankton genus. Using a two-component PLS-DA model, viable and nonviable cells can be clearly classified with sensitivities and specificities ≥95%. In addition, the multivariate statistical analysis of the spectra revealed changes in the molecular signatures of other pigments as well as those of proteins and lipids. This addresses two major issues in the applicability of this technique to rapid on-site monitoring of changes in phytoplankton communities. This work paves the way for the further investigation of a more diverse population of phytoplankton to determine whether these biomarkers show similar trends in phytoplankton with different major chlorophyll and carotenoid pigment compositions.

EXPERIMENTAL SECTION

Cell Preparation. *Tisochrysislutea*, *Diacronemalutheri*, and *Chaetocerosmuelleri* phytoplankton were sourced from CSIRO Tasmania and grown in artificial seawater with a F/2 media mixture. The cultures were illuminated at a photosynthetic photon flux density (PPFD) of 47 μmol cm^{-2} s^{-1}, a color temperature of 8603 K, and a flux of 1297 lm mm^{-2} at average temperatures of 18−20 °C. Air was con stantly bubbled into the mixture. To test for spectral changes due to viability, phytoplankton samples were collected, and two measurements

https://doi.org/10.1021/acsomega.1c06262
ACS Omega 2022, 7, 5962−5971

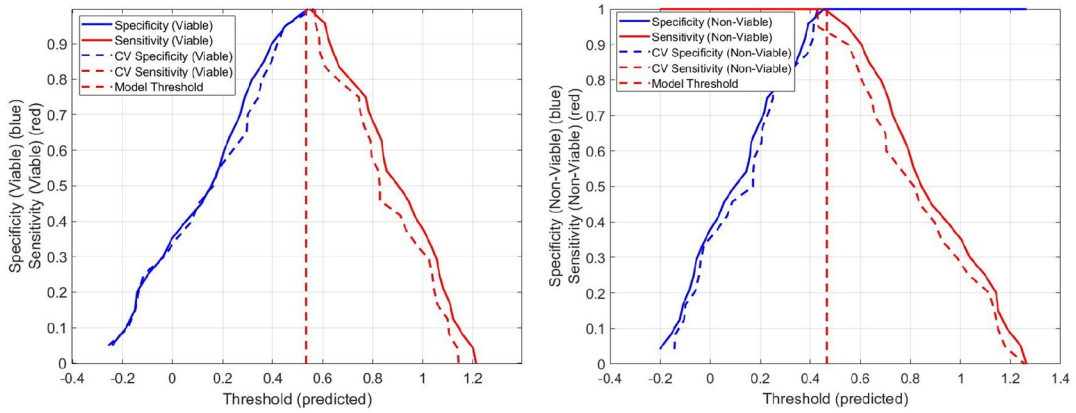

Figure 9. Estimated (solid) and cross-validated (CV) (dashed) responses for viable and heat-treated cells together with the model threshold.

PLS-DA Cross validation		
Class	Sensitivity	Specificity
Viable	0.95	1
Non-Viable	1	0.95

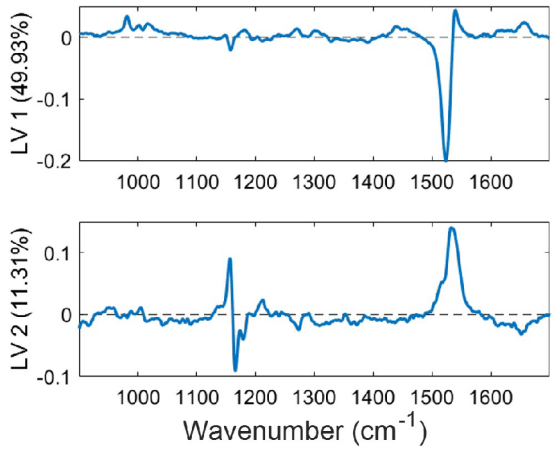

Figure 10. Cross-validated classification results of the PLS-DA. High sensitivity and specificity were achieved using the first two latent variables shown (LV1 and LV2).

were made (1) immediately after collection and 2) after cells were heat-treated at 60°C for 10 min in a water bath.

Raman Spectroscopy. *In situ* Raman measurements of the phytoplankton cells were carried out in an artificial seawater solution on an aluminum foil-covered Petri dish coated with poly L-lysine polymer. Cells were allowed to settle and adhere to the polymer coating prior to measurement. Raman spectra were acquired in the backscattering geometry using a LabRAM HR Evolution Raman confocal microscope and a 40× water immersion objective with NA = 0.80. The spot size of the laser at focal point was 12.5 μm, and the confocal pinhole set to 1000 μm. The depth of focus was calculated at 230.7 μm with a measured effective volume of 28 307.9 μm^3. The excitation radiation used was a 1064 nm solid-state laser at a power of 80 mW measured in air. The system was comprised of a liquid N_2-cooled Linear InGaAs array detector of 512 pixels, a 600 gr mm^{-1} (750 nm) blazed grating, and a holographic notch filter to remove Rayleigh scattered light. The Raman spectra were acquired over the range of 900−1700 cm^{-1} with acquisition times ranging between 90 and 180 s to maximize the signal intensity. The spectra were stable over long irradiation times, indicating that the laser power used did not cause degradation during the experiment. Each species was measured between 20 and 24 times, each at a different spot, to give a total of 66 spectra.

Spectral Preprocessing. Spectra were smoothed using a Savitsky−Golay algorithm (with a second-order polynomial and 15 adjacent point averaging), baseline-corrected using an automatic Whittaker filter (asymmetry of 0.005 and λ set to 5 × 10^6), area-normalized, and mean-centered prior to building the PCA model. All the preprocessing steps were carried out using PLS Toolbox (Eigenvector Research).

Multivariate Data Analysis. The PCA of the data was carried out on the PLS Toolbox (Eigenvector Research). The resulting spectral variances were used to discriminate differences among the different species and the viability of cells. For classification purposes, PLS-DA was performed, also using the PLS Toolbox (eigenvector Research).

Excitation Spectroscopy. Excitation spectra were measured using a Jasco FP-8600 fluorescence spectrometer at 680 nm; this emission wavelength corresponds to the chlorophyll emission band. The spectra were acquired between 200 and 850 nm at 5 nm data intervals and 5 nm excitation and emission slit widths.

AUTHOR INFORMATION

Corresponding Author

Nina I. Novikova − *School of Chemical Sciences, University of Auckland, Auckland 1010, New Zealand; The Photon Factory, University of Auckland, Auckland 1010, New Zealand; The Dodd-Walls Centre for Photonic and Quantum Technologies, Dunedin 9016, New Zealand; MacDiarmid Institute for Advanced Materials and Nanotechnology, Wellington 6011, New Zealand;* Present Address: 23 Symonds Street, Auckland 1010, New Zealand; orcid.org/0000-0001-7469-5878; Email: nina.novikova@auckland.ac.nz

Authors

Hannah Matthews − *School of Chemical Sciences, University of Auckland, Auckland 1010, New Zealand; The Photon Factory, University of Auckland, Auckland 1010, New Zealand; The Dodd-Walls Centre for Photonic and Quantum Technologies, Dunedin 9016, New Zealand; MacDiarmid Institute for Advanced Materials and Nanotechnology, Wellington 6011, New Zealand*

https://doi.org/10.1021/acsomega.1c06262
ACS Omega 2022, 7, 5962−5971

Isabelle Williams − *School of Chemical Sciences, University of Auckland, Auckland 1010, New Zealand; The Photon Factory, University of Auckland, Auckland 1010, New Zealand; The Dodd-Walls Centre for Photonic and Quantum Technologies, Dunedin 9016, New Zealand; MacDiarmid Institute for Advanced Materials and Nanotechnology, Wellington 6011, New Zealand*

Mary A. Sewell − *School of Biological Sciences, University of Auckland, Auckland 1010, New Zealand*

Michel K. Nieuwoudt − *School of Chemical Sciences, University of Auckland, Auckland 1010, New Zealand; The Photon Factory, University of Auckland, Auckland 1010, New Zealand; The Dodd-Walls Centre for Photonic and Quantum Technologies, Dunedin 9016, New Zealand; MacDiarmid Institute for Advanced Materials and Nanotechnology, Wellington 6011, New Zealand*

M. Cather Simpson − *School of Chemical Sciences, University of Auckland, Auckland 1010, New Zealand; The Photon Factory, University of Auckland, Auckland 1010, New Zealand; The Dodd-Walls Centre for Photonic and Quantum Technologies, Dunedin 9016, New Zealand; MacDiarmid Institute for Advanced Materials and Nanotechnology, Wellington 6011, New Zealand;* orcid.org/0000-0001-9624-4947

Neil G. R. Broderick − *Department of Physics, University of Auckland, Auckland 1010, New Zealand; The Photon Factory, University of Auckland, Auckland 1010, New Zealand; The Dodd-Walls Centre for Photonic and Quantum Technologies, Dunedin 9016, New Zealand*

Complete contact information is available at: https://pubs.acs.org/10.1021/acsomega.1c06262

Notes

The authors declare no competing financial interest.

■ ACKNOWLEDGMENTS

The authors thank Ministry of Business, Innovation, and Employment for funding this Science for Technology and Innovation (SfTI) spearhead project. The authors acknowledge Cawthron Institute for sharing their expertise in phytoplankton growth and handling. The authors also thank Dr. Andrew Jeffs from the Institute of Marine Science and School of Biological Sciences at the University of Auckland for supplying the *T. lutea*, *D. lutheri*, and *C. muelleri* cultures. Phytoplankton and protein images in the TOC were adapted from BioRender.com (2021) and retrieved from https://app.biorender.com/biorender-templates.

■ REFERENCES

(1) Falkowski, P. G.; Katz, M. E.; Knoll, A. H.; Quigg, A.; Raven, J. A.; Schofield, O.; Taylor, F. J. R. The Evolution of Modern Eukaryotic Phytoplankton. *Science* **2004**, *305*, 354−360.

(2) Falkowski, P. G. Ocean Science: The power of plankton. *Nature* **2012**, *483*, S17−S20.

(3) Law, C. S.; Rickard, G. J.; Mikaloff-Fletcher, S. E.; Pinkerton, M. H.; Behrens, E.; Chiswell, S. M.; Currie, K. Climate change projections for the surface ocean around New Zealand. *New Zealand Journal of Marine and Freshwater Research* **2018**, *52*, 309−335.

(4) Pahlevan, N.; Smith, B.; Binding, C.; Gurlin, D.; Li, L.; Bresciani, M.; Giardino, C. Hyperspectral retrievals of phytoplankton absorption and chlorophyll-a in inland and nearshore coastal waters. *Remote Sensing of Environment* **2021**, *253*, 112200.

(5) Anderson, D. M.; Cembella, A. D.; Hallegraeff, G. M. Progress in understanding harmful algal blooms: Paradigm shifts and new technologies for research, monitoring, and management. *Ann. Rev. Mar Sci.* **2012**, *4*, 143−176.

(6) Babichenko, S.; Leeben, A.; Poryvkina, L.; van der Wagt, R.; de Vos, F. Fluorescent screening of phytoplankton and organic compounds in sea water. *J. Environ. Monit.* **2000**, *2*, 378−383.

(7) Sosik, H. M.; Olson, R. J. Automated taxonomic classification of phytoplankton sampled with imaging-in-flow cytometry. *Limnology and Oceanography: Methods* **2007**, *5*, 204−216.

(8) Li, H.-P.; Gong, G.-C.; Hsiung, T.-M. Phytoplankton pigment analysis by HPLC and its application in algal community investigations. *Bot. Bull. Acad. Sin.* **2002**, *43*, 283−290.

(9) Biller, P.; Ross, A. Pyrolysis GC−MS as a novel analysis technique to determine the biochemical composition of microalgae. *Algal Research* **2014**, *6*, 91−97.

(10) Crupi, P.; Toci, A. T.; Mangini, S.; Wrubl, F.; Rodolfi, L.; Tredici, M. R.; Coletta, A.; Antonacci, D. Determination of fucoxanthin isomers in microalgae (Isochrysis sp.) by high-performance liquid chromatography coupled with diode-array detector multistage mass spectrometry coupled with positive electrospray ionization. *Rapid Commun. Mass Spectrom.* **2013**, *27*, 1027−1035.

(11) Heraud, P.; Beardall, J.; McNaughton, D.; Wood, B. R. In vivo prediction of the nutrient status of individual microalgal cells using Raman microspectroscopy. *FEMS Microbiology Letters* **2007**, *275*, 24−30.

(12) Kuhar, N.; Sil, S.; Verma, T.; Umapathy, S. Challenges in application of Raman spectroscopy to biology and materials. *RSC Adv.* **2018**, *8*, 25888−25908.

(13) De Gelder, J.; De Gussem, K.; Vandenabeele, P.; Moens, L. Reference database of Raman spectra of biological molecules. *J. Raman Spectrosc.* **2007**, *38*, 1133−1147.

(14) Novikova, N. I.; Lo, A. S. V.; Gordon, K. C.; Brothers, P. J.; Simpson, M. C. Diboron Porphyrins: The Raman Signature of the In-Plane Tetragonal Elongation of the Macrocycle. *J. Phys. Chem. A* **2018**, *122*, 5121−5131. PMID: 29745659.

(15) Samek, O.; Jonáš, A.; Pilat, Z.; Zemanek, P.; Nedbal, L.; Triska, J.; Kotas, P.; Trtilek, M. Raman Microspectroscopy of Individual Algal Cells: Sensing Unsaturation of Storage Lipids in vivo. *Sensors (Basel, Switzerland)* **2010**, *10*, 8635−8651.

(16) Wu, H.; Volponi, J. V.; Oliver, A. E.; Parikh, A. N.; Simmons, B. A.; Singh, S. In vivo lipidomics using single-cell Raman spectroscopy. *Proc. Natl. Acad. Sci. U. S. A.* **2011**, *108*, 3809−3814.

(17) Andreasen, M.; Lundgreen, K.; Holbech, H.; Hedegaard, M. A. Raman spectroscopy as a tool for viability assessment of planktonic organisms in UV treated ballast water. *Vib. Spectrosc.* **2020**, *110*, 103142.

(18) He, S.; Xie, W.; Zhang, P.; Fang, S.; Li, Z.; Tang, P.; Gao, X.; Guo, J.; Tlili, C.; Wang, D. Preliminary identification of unicellular algal genus by using combined confocal resonance Raman spectroscopy with PCA and DPLS analysis. *Spectrochimica Acta Part A: Molecular and Biomolecular Spectroscopy* **2018**, *190*, 417−422.

(19) Barletta, R. E.; Krause, J. W.; Goodie, T.; El Sabae, H. The direct measurement of intracellular pigments in phytoplankton using resonance Raman spectroscopy. *Marine Chemistry* **2015**, *176*, 164−173.

(20) Jehlicka, J.; Edwards, H. G.; Osterrothova, K.; Novotna, J.; Nedbalova, L.; Kopecky, J.; Nemec, I.; Oren, A. Potential and limits of Raman spectroscopy for carotenoid detection in microorganisms: implications for astrobiology. *Philosophical Transactions of the Royal Society A: Mathematical, Physical and Engineering Sciences* **2014**, *372*, 20140199.

(21) Wei, D.; Chen, S.; Liu, Q. Review of Fluorescence Suppression Techniques in Raman Spectroscopy. *Appl. Spectrosc. Rev.* **2015**, *50*, 387−406.

(22) Hoskins, L. C.; Alexander, V. Determination of carotenoid concentrations in marine phytoplankton by resonance Raman spectrometry. *Anal. Chem.* **1977**, *49*, 695−697. PMID: 855913.

(23) Gautam, R.; Vanga, S.; Ariese, F.; Umapathy, S. Review of multidimensional data processing approaches for Raman and infrared spectroscopy. *EPJ. Tech. Instrum.* **2015**, *2*, 8.

(24) Nieuwoudt, M. K.; Shahlori, R.; Naot, D.; Patel, R.; Holtkamp, H.; Aguergaray, C.; Watson, M.; Musson, D.; Brown, C.; Dalbeth, N.; et al. Raman spectroscopy reveals age-and sex-related differences in cortical bone from people with osteoarthritis. *Sci. Rep.* **2020**, *10*, 19443.
(25) Nieuwoudt, M.; Holroyd, S.; McGoverin, C.; Simpson, M.; Williams, D. Raman spectroscopy as an effective screening method for detecting adulteration of milk with small nitrogen-rich molecules and sucrose. *Journal of dairy science* **2016**, *99*, 2520−2536.
(26) Ahmmed, F.; Fraser-Miller, S. J.; Garagoda Arachchige, P. S.; Schallenberg, M.; Novis, P.; Gordon, K. C. Lake snow caused by the invasive diatom *Lindavia intermedia* can be discriminated from different sites and from other algae using vibrational spectroscopy. *J. Raman Spectrosc.* **2021**, *52*, 2597.
(27) Pi, X.; Zhao, S.; Wang, W.; Liu, D.; Xu, C.; Han, G.; Kuang, T.; Sui, S.-F.; Shen, J.-R. The pigment-protein network of a diatom photosystem II−light-harvesting antenna supercomplex. *Science* **2019**, *365*, eaax4406.
(28) Wang, W.; Yu, L.-J.; Xu, C.; Tomizaki, T.; Zhao, S.; Umena, Y.; Chen, X.; Qin, X.; Xin, Y.; Suga, M. Structural basis for blue-green light harvesting and energy dissipation in diatoms. *Science* **2019**, *363*, eaav0365.
(29) Geider, R. J.; Moore, C. M.; Suggett, D. J. Ecology of Marine Phytoplankton. In *Ecology and the Environment*; Monson, R. K., Ed.; Springer New York: New York, NY, 2014; pp 483−531.
(30) Ragueneau, O.; de Bias Varela, E.; Tréguer, P.; Quéguiner, B.; Del Amo, Y. Phytoplankton dynamics in relation to biogeochemical cycle of silicon in a coastal ecosystem of Western Europe. *Mar. Ecol. Prog. Ser.* **1994**, *106*, 157−172.
(31) Hallegraeff, G. M. Ocean Climate Change, phytoplankton community responses, and harmful algal blooms: a formidable predictable predictive challenge. *Journal of Phycology* **2010**, *46*, 220−235.
(32) Green, M. A.; Aller, R. C. Seasonal patterns of carbonate diagenesis in nearshore terrigenous muds: Relation to spring phytoplankton bloom and temperature. *Journal of Marine Research* **1998**, *56*, 1097−1123.
(33) Hastuti, A. W.; Pancawati, Y.; Surana, I. N. The abundance and spatial distribution of plankton communities in Perancak Estuary, Bali. *IOP Conference Series: Earth and Environmental Science* **2018**, *176*, 012042.
(34) Movasaghi, Z.; Rehman, S.; Rehman, D. I. U. Raman Spectroscopy of Biological Tissues. *Appl. Spectrosc. Rev.* **2007**, *42*, 493−541.
(35) Koyama, Y.; Umemoto, Y.; Akamatsu, A.; Uehara, K.; Tanaka, M. Raman spectra of chlorophyll forms. *J. Mol. Struct.* **1986**, *146*, 273−287.
(36) Withnall, R.; Chowdhry, B. Z.; Silver, J.; Edwards, H. G.; de Oliveira, L. F. Raman spectra of carotenoids in natural products. *Spectrochimica acta part a: molecular and biomolecular spectroscopy* **2003**, *59*, 2207−2212.
(37) Barletta, R. E.; Krause, J. W.; Goodie, T.; El Sabae, H. The direct measurement of intracellular pigments in phytoplankton using resonance Raman spectroscopy. *Marine Chemistry* **2015**, *176*, 164−173.
(38) Wu, H.; Volponi, J. V.; Oliver, A. E.; Parikh, A. N.; Simmons, B. A.; Singh, S. In vivo lipidomics using single-cell Raman spectroscopy. *Proc. Natl. Acad. Sci. U. S. A.* **2011**, *108*, 3809−3814.
(39) Moudrikova, S.; Sadowsky, A.; Metzger, S.; Nedbal, L.; Mettler-Altmann, T.; Mojzeš, P. Quantification of polyphosphate in microalgae by Raman microscopy and by a reference enzymatic assay. *Analytical chemistry* **2017**, *89*, 12006−12013.
(40) Falkowski, P. G.; Katz, M. E.; Knoll, A. H.; Quigg, A.; Raven, J. A.; Schofield, O.; Taylor, F. The evolution of modern eukaryotic phytoplankton. *science* **2004**, *305*, 354−360.
(41) McGinnis, K.; Dempster, T.; Sommerfeld, M. Characterization of the growth and lipid content of the diatom Chaetoceros muelleri. *Journal of Applied Phycology* **1997**, *9*, 19−24.

https://doi.org/10.1021/acsomega.1c06262
ACS Omega 2022, 7, 5962−5971